*materials*

MDPI

*Review*

# The Review of Hybridization of Transition Metal-Based Chalcogenides for Lithium-Ion Battery Anodes

**Lin-Hui Wang [1], Long-Long Ren [2] and Yu-Feng Qin [1,*]**

[1] College of Information Science and Engineering, Shandong Agricultural University, Taian 271018, China
[2] College of Mechanical and Electronic Engineering, Shandong Agricultural University, Taian 271018, China
* Correspondence: qinyufeng@sdau.edu.cn

**Abstract:** Transition metal chalcogenides as potential anodes for lithium-ion batteries have been widely investigated. For practical application, the drawbacks of low conductivity and volume expansion should be further overcome. Besides the two conventional methods of nanostructure design and the doping of carbon-based materials, the component hybridization of transition metal-based chalcogenides can effectively enhance the electrochemical performance owing to the synergetic effect. Hybridization could promote the advantages of each chalcogenide and suppress the disadvantages of each chalcogenide to some extent. In this review, we focus on the four different types of component hybridization and the excellent electrochemical performance that originated from hybridization. The exciting problems of hybridization and the possibility of studying structural hybridization were also discussed. The binary and ternary transition metal-based chalcogenides are more promising to be used as future anodes of lithium-ion batteries for their excellent electrochemical performance originating from the synergetic effect.

**Keywords:** transition metal; chalcogenides; anodes; lithium-ion batteries; hybridization; synergetic effect

check for updates

**Citation:** Wang, L.-H.; Ren, L.-L.; Qin, Y.-F. The Review of Hybridization of Transition Metal-Based Chalcogenides for Lithium-Ion Battery Anodes. *Materials* **2023**, *16*, 4448. https://doi.org/10.3390/ma16124448

Academic Editor: Giovanni Battista Appetecchi

Received: 31 March 2023
Revised: 5 June 2023
Accepted: 15 June 2023
Published: 18 June 2023

**Copyright:** © 2023 by the authors. Licensee MDPI, Basel, Switzerland. This article is an open access article distributed under the terms and conditions of the Creative Commons Attribution (CC BY) license (https://creativecommons.org/licenses/by/4.0/).

## 1. Introduction

With the increasingly serious energy crisis, more and more attention has been paid to green energies, such as wind energy and solar energy [1,2]. To resolve the disadvantages of the intermittency and randomness of these green energies, the development of energy conversion and storage systems is becoming increasingly significant. Lithium-ion batteries (LIBs) have been widely explored and applied in portable electronics, electric vehicles, and high-power energy storage systems, on account of their long cycle life, and high specific capacity [3,4]. However, traditional carbon-based anodes are facing the challenges of improving the energy density and rate performance raised by high-power energy storage systems and artificial intelligence vehicles [5,6]. Despite the advantages of abundance, relatively low lithiation voltage, and high lithium storage for the alloying anodes, such as Si-based, Ge-based, and Sn-based materials, the large destructive effects of volumetric expansion during cycling and low intrinsic electronic conductivity prohibit the further application of these alloying anodes [7–9].

As a representative of the conversion reaction, transition metal chalcogenides, as one of the most promising alternatives to carbon-based anodes, have been extensively explored, exhibiting high specific capacity and outstanding rate performance [10–12]. For practical application, the drawbacks of volume expansion and low conductivity for these anode materials during the cycling process should be further resolved. Therefore, diverse nanostructures have been designed and prepared using many preparation methods. The nanostructures can increase the specific surface and decrease the intercalation path, and therefore increase the specific capacity of the transition metal chalcogenide anodes [13–17]. Cubic hollow CuS nano-boxes anodes exhibited superior cycle stability and high specific capacity at 20 C [13]. Synthesized by a sol-gel method, CuS nanorods achieved excellent

cycle stability and high Coulombic efficiency [14]. Hu et al. synthesized CuS porous spheres and hollow spheres by a bubble template method, which indicated a promising alternative to carbon-based anodes for LIBs [15]. CuO anodes showed excellent electrochemical performance due to the unique morphology of the leaf-like nanoplates [16]. The core/shell-structured NiS anodes were prepared by the arc discharge method and exhibited good cyclability, high capacity, and outstanding rate capability [17]. Besides, carbon-based materials, such as graphene, reduced graphene oxide (rGO), and graphite, have been generally introduced to transition metal chalcogenides anodes. The introduction of carbon-based materials can enhance the cycle stability and conductivity of transition metal chalcogenide anodes to some extent [18–23]. In the rGO matrix, $Fe_3S_4$ nanoparticles were obtained by a one-pot hydrothermal method, showing excellent specific capacity and high conductivity [18]. The tubular mesoporous carbon materials were introduced to prepare $Cu_2S$/C nanocomposites, which showed relatively good reversible capacity and rate capability [19]. CuS/CNTs nanocomposites were synthesized by a solvothermal method and exhibited good electrochemical performance due to the synergetic effect between carbon nanotubes and CuS [20]. CuO/graphene nanomaterials possessed an enhanced accommodation of lithium ions intercalation due to the synergetic effect of graphene [21]. Graphene with different structures was also introduced to $Mn_3O_4$ nanomaterials, which enhanced the conducive network and cycle stability of the anode materials [22,23].

In addition to the two above-mentioned solutions, the hybridization of transition metal-based chalcogenide anodes was reported, which could effectively enhance the electrochemical performance because of the synergetic effect of diverse components. The multifunctional component hybridization of the anode materials should be an effective way to accomplish excellent electrochemical performance for transition metal chalcogenides. It is worth noting that "hybridization" does not mean a simple mixture composed of two or more materials but a hybrid material with chemical links between each other in which the electronic structure of the hybrid material itself will be different from the mixture. Many works and reviews were reported based on the investigation of nanostructure designing and carbon-based material doping [13–23]. As far as we know, there are many studies on hybridization, but a summary of hybridization has not been reported. Generally, the hybridization can be divided into the hybridization between the transition metal and the transition metal chalcogenide, and the hybridization between different transition metal chalcogenides. In this review, we concentrate on the four types of hybridization, by which the individual advantages of each component could be strengthened and excellent electrochemical performance could be obtained. We also discuss the exciting problems of hybridization and the possibility of studying structural hybridization.

## 2. Hybridization between the Transition Metal and Transition Metal Chalcogenide

Because of the high conductivity and the catalytic property for the decomposition of $Li_2O$, transition metal doping has been investigated, and the enhanced electrochemical performance of transition metal chalcogenide anodes was obtained. Generally, transition metal doping includes the hybridization of X and X-chalcogenides, and the hybridization of X and Y-chalcogenides, in which X and Y denote different transition metals, while X-chalcogenide and Y-chalcogenide represent different transition metal chalcogenides.

### *2.1. Hybridization of X and X-Chalcogenides*

The transition metal could not only catalyze the reversible decomposition of $Li_2O$ but also help to establish the conductive network in the hybrid electrodes. The hybridization of a transition metal and the same metal-based chalcogenide was always achieved by accurately controlling the oxidation or reduction process.

Compared to pure CoO, the core-shell nanostructured Co@CoO exhibited superior electrochemical performance due to the existence of Co metal. According to their catalytic ability, the core Co metal nanoparticles could enhance the reversible decomposition of $Li_2O$, while the outside Co metal portion could establish the conductivity network between

the CoO anode materials [24]. Hao et al. prepared Co/CoO nanoparticles anchored on porous carbon cuboids by an impregnation method and consequent high-temperature treatment. Due to the synergetic effect between Co and CoO, as well as the unique hierarchical structure, the PCC-CoO*x* anodes showed high specific capability, long cycle life, and outstanding rate capability at high current density [25]. The Co/CoO@N-C nanocomposites were obtained by a facile chemical process and exhibited an enhanced initial capacity and a relatively high reversible specific capacity. The remarkable electrochemical performance originated from the increased conductivity and enhanced catalytic effect on $Li_2O$, which were induced by heterogeneous composite doping [26]. $Co_3O_4$@CoO@Co nanocomposites were prepared by the hydrothermal method and following calcination treatment. The $Co_3O_4$@CoO@Co nanomaterials exhibited superior electrochemical and catalytic performance in the fields of LIBs and oxygen evolution reactions due to the modification of these components with each other [27]. Owing to the enhanced stability and improved conductivity achieved by the doping of metal Cu, the $Cu_2O$/Cu nanowires exhibited greater remarkable cyclability and much higher capacity than conventional pure $Cu_2O$ [28]. The sub-microsphere structured $Cu_2O$@Cu composites showed an outstanding rate performance and good cycling performance, which was ascribed to the synergistic effect between the volume-buffering capacity and the high electronic conductivity of metallic Cu in $Cu_2O$@Cu composites [29]. The metallic Cu in $Cu_2O$ could act as a conducting way for electrons, a volume buffer during the cycling process, and a catalyst for the decomposition of $Li_2O$. Wang et al. successfully synthesized core-shell structured Cu/$Cu_2O$@Ppy nanowires by a one-step hydrothermal method, showing superior Li-storage performance caused by the nanowires' structure and the introduction of Cu metal. In the anode materials, Cu metal could enhance the conductivity and the electrochemical reaction kinetics [30]. The nanostructured NiS/Ni electrode was prepared and showed high specific capacity and long cycle life resulting from the special porous structure and the formation of a conductivity network by Ni in the materials [31]. Zhu et al. explored a highly efficient and facile milling strategy to prepare Sn@SnO*x*/C nanocomposites. The Sn@SnO*x*/C anodes exhibited a stable reversible capacity after many cycles due to the amorphous microstructure and the conductive network established by the Sn nanoparticles [32]. The better electrochemical performance of a hybrid of X and X-chalcogenides than pure transition metal chalcogenide can be seen in Table 1 and Figure 1 [26,30].

**Table 1.** The electrochemical performance comparison of X and X-Chalcogenides hybrid materials and pure materials.

| **Hybrid Materials Capacity [mAh $g^{-1}$]** | | **Pure Materials Capacity [mAh $g^{-1}$]** | | **Current [mA $g^{-1}$]** | **Refs.** |
|---|---|---|---|---|---|
| Co@CoO | 800 (50 cycles) | CoO | 200 (50 cycles) | 50 | [24] |
| PCC-$CoO_x$ | 618 (500 cycles) | CoO | 452 (500 cycles) | 500 | [25] |
| Co/CoO@N-C | 1115 (125 cycles) | CoO | 718 (125 cycles) | 200 | [26] |
| Cu/$Cu_2O$@Ppy | 787 (250 cycles) | $Cu_2O$@Ppy | 200 (140 cycles) | 100 | [30] |
| Sn@$SnO_x$/C | 430 (200 cycles) | Sn-$SnO_2$-C | 300 (200 cycles) | 250 | [32] |

### *2.2. Hybridization of X and Y-Chalcogenide*

Compared to homoatomic metal doping, heteroatom hybridization could be easily accomplished by controlling the kinds and ratios of the chemical precursors. The hybrid of transition metal chalcogenide and heteroatoms tended to exhibit more remarkable electrochemical performance than pure transition metal chalcogenide.

Wang et al. found that the concentration of the doped Cu could regularly affect the morphologies and structures of the CoO/Cu nanocomposites. At a certain concentration, the CoO/Cu nanocomposites showed remarkable cycling stability to 1000 cycles and a high specific capacity of 580 mAh/g at 10 C, which are much better than pure CoO nanomaterials [33]. The outstanding electrochemical performance of the CoO/Cu anodes originated from the improved electron conductivity, enhanced catalytic function, and significant

structure stability of CoO/Cu induced by Cu doping. The structure, morphologies, and electrochemical performance of a series of Ce-doped $Mn_3O_4$ nanocrystals with different Ce concentrations were thoroughly investigated. $Mn_{2.98}Ce_{0.02}O_4$ anodes exhibited the highest capacity of 754.2 mAh/g up to 100 cycles, which was attributed to the bigger diffusion channels, more robust structure, and lower charge transfer impedance induced by the doping of Ce [34]. Krishnan et al. proposed a simple, environmentally friendly, and low-cost method to synthesize Mo-doped $Cu_2O$:Mo with a porous microsphere structure. The remarkable electrochemical performance of the $Cu_2O$:Mo anodes originated from the improvement of the specific surface area, electrical conductivity, Li-ion transports, and electrochemical kinetics induced by Mo doping [35]. The Zn-doped $Co_3O_4$ nanocomposites with a hollow concave structure displayed excellent rate capability and high specific capacities with stable cyclability. The outstanding electrochemical performance originated from the unique hollow concave structure and the defects induced by Zn doping, which could effectively improve the electronic structure of $Co_3O_4$ composites and then enhance the electrochemical reaction kinetics [36]. Wu et al. reported that the binary transition metal $Cu_{3.8}Ni$ was doped with CoO and MnO. The obtained $Cu_{3.8}Ni$/CoO and $Cu_{3.8}Ni$/MnO nanocomposites exhibited long cycle life, high energy density, and high power density, resulting from the establishment of the electron carrier path by $Cu_{3.8}Ni$ doping. [37].

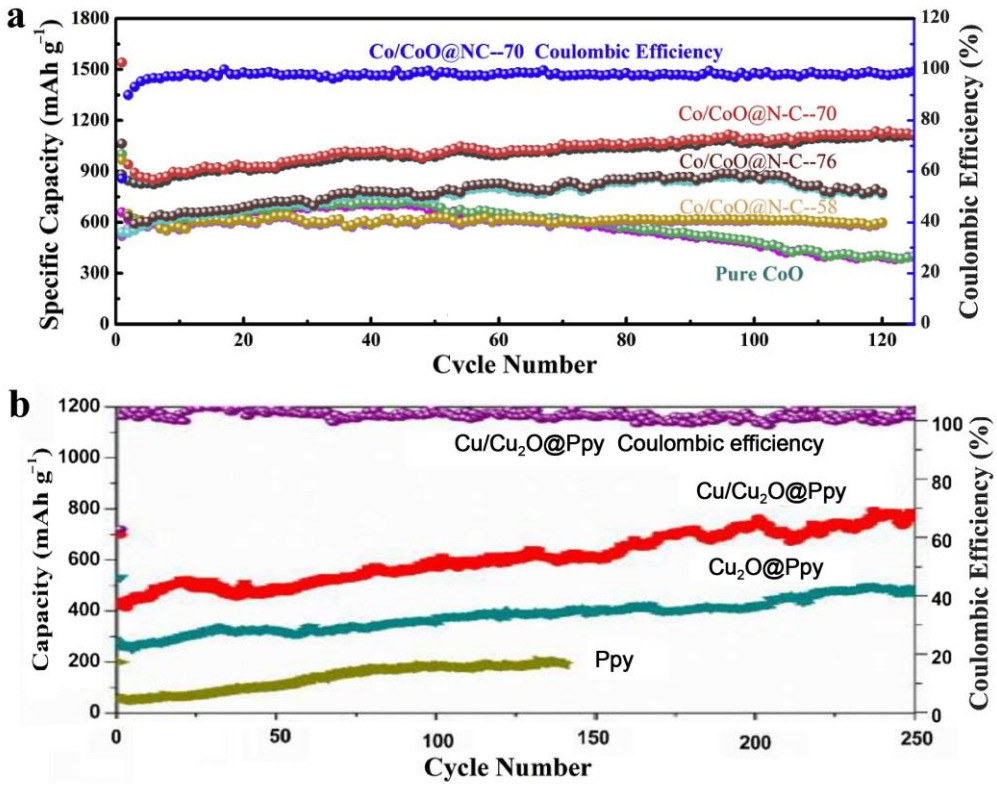



**Figure 1.** (**a**) Comparison of Co/CoO@N-C and pure CoO at 200 mA/g [26]. (**b**) Comparison of Cu/$Cu_2O$@Ppy, $Cu_2O$@Ppy, and pure Ppy at 100 mA/g [30].

Other metal-doped compound anodes for lithium-ion batteries were also reported. The physical properties and electrochemical performance of Mn-doped $Co_2(OH)_3Cl$ xerogels depending on the Mn concentration were systematically investigated. Compared to pure $Co_2(OH)_3Cl$, the 4% Mn-doped $Co_2(OH)_3Cl$ xerogels displayed a superior capacity and an outstanding rate capability, which could be mainly ascribed to the increased electric conductivity and charge transfer ability induced by Mn doping [38]. Through a ball milling activating technique, $Li_4Ti_{5-x}Y_xO_{12}$ anode materials were obtained by Y doping to $Li_4Ti_5O_{12}$ and exhibited fast diffusion of lithium ions, outstanding rate capability, and excellent long-cycle stability. The introduction of hetero valence Y can establish a new

charge balance with the spinel structure unchanged, by which the Li diffusion coefficient, electrical conductivity, and electrochemical performances were improved [39]. The better electrochemical performance of the hybrid of X and Y-chalcogenide than pure transition metal chalcogenide was summarized in Table 2.

**Table 2.** The electrochemical performance comparison of X and Y-Chalcogenide hybrid materials and pure materials.

| Hybrid Materials Capacity [mAh $g^{-1}$] | | Pure Materials Capacity [mAh $g^{-1}$] | | Current [mA $g^{-1}$] | Refs. |
|---|---|---|---|---|---|
| $Co_{0.95}Cu_{0.05}O$ | 800 (80 cycles) | CoO | 500 (200 cycles) | 0.5 C | [33] |
| $Mn_{2.98}Ce_{0.02}O_4$ | 754.2 (100 cycles) | $Mn_3O_4$ | 306 (100 cycles) | 100 | [34] |
| $Cu_2O$:Mo | 1122 (100 cycles) | $Cu_2O$ | 820 (100 cycles) | 100 | [35] |
| $Mn/Co_2(OH)_3Cl$ | 1377 (50 cycles) | $Co_2(OH)_3Cl$ | 277 (50 cycles) | 100 | [38] |

## 3. Hybridization between Different Transition Metal Chalcogenides

Recently, many binary and ternary transition metal chalcogenides have been prepared and exhibited outstanding electrochemical performance. The hybridization of transition metal chalcogenides could promote the advantages of each chalcogenide and suppress the disadvantages of each chalcogenide. Therefore, the excellent electrochemical performance of a hybrid of transition metal chalcogenides could be obtained on account of the synergetic effect.

### *3.1. Hybridization of X-Chalcogenide and X-Chalcogenide*

Due to the multivalent state of the transition metals, the two phrases of X-chalcogenide in the above title represent two different X-based chalcogenides, such as CoO and $Co_3O_4$, MnO and $Mn_3O_4$, CuO and $Cu_2O$. Therefore, the hybridization of the same transition metal-based but different chalcogenides is discussed in this part.

Zhu et al. prepared dandelion-like $CoO/Co_3O_4/C$ nanocomposites by a hydrothermal method and the following unique combustion method. The $CoO/Co_3O_4/C$ anodes exhibited stable and high capacity at different current densities [40]. Prepared by a hydrothermal reaction and a subsequent calcination and reduction process, porous $Co_3O_4$@CoO nanosheet anodes showed an outstanding rate capability even at 5 A/g and an excellent specific capacity [41]. Li et al. synthesized $Co(OH)_2/Co_3O_4/Co$ nanoparticles derived from the EDTA-Co(II) sodium complex. The anode materials exhibited a high reversible capacity, good cycling stability, and high-rate performance, which originated from the porous structure, the presence of conductive Co, and especially the synergetic effect of $Co(OH)_2$ and $Co_3O_4$ [42]. The $MnO/Mn_3O_4$@NC composites with a porous structure were prepared and used as anodes of LIBs. The relatively high electrochemical performance resulted from the special porous structure and the co-doping of N and Mn [43]. After 630 cycles, the $MnO/Mn_3O_4/SeO_x$ ($x$ = 0, 2) hybrid anodes exhibited a reversible specific capacity of up to 1007 mAh/g at 3 A/g, resulting from the synergetic effect between MnO and $Mn_3O_4$ phases [44]. Grown on conductive collectors of β-NiS@$Ni_3S_2$, the bind-free anodes of NiO nanosheet arrays exhibited outstanding lithium storage properties owing to the special heterostructures and the synergetic effect of the $Ni_3S_2$, β-NiS, and NiO components [45]. The $CuS/Cu_{1.8}S$ nanocomposite anodes showed a better electrochemical performance than that of most of the previous reports, owing to the nano-size structure and the assistance of the $Cu_{1.8}S$ component [46].

Yolk–shell structured $Cu_2O$@CuO nanocomposites were prepared by a multistep chemical method at room temperature. The anode nanocomposites exhibited superior cycling stability and rate capability with a reversible capacity of up to 854 mAh/g at 0.1 C after 200 cycles, which could be mostly attributed to the improved conductivity induced by the spur-CuO bridge and CuO shell [47]. Quaternary $Cu_2O/CuO/Cu$/Carbon-polymer composite fibers were obtained and exhibited good rate performance, excellent cycle stabil-

ity, and high capacity due to the fiber structure and the combination of metal and metal oxides [48]. Compared to pure CuO nanowires, the $CuO/Cu_2O/Cu$ exhibited much better electrochemical performance, which was ascribed to the synergetic effect of the ternary composites [49]. The outstanding electrochemical performance of the $CuO/Cu_2O/C$ anodes with uniform spherical morphology was attributed to the synergetic effect of the two-component $CuO/Cu_2O$, porous structure, and conducting carbon coating [50]. Ternary $CuO/Cu_2O/Cu$ composites were designed and prepared by a method of electrodeposition and following calcination in air. The obtained bind-free $CuO/Cu_2O/Cu$ anodes displayed a high capacity, which originated from the cypress-like structure and the synergetic effect between the conductive Cu and the active Cu oxides [51]. Used in lithium/sodium-ion batteries, the $CuO/Cu_2O$ anodes anchored in graphite matrix exhibited high capacity and cycling stability, mainly due to the synergetic effect of the CuO and $Cu_2O$ nanoparticles [52]. Other $CuO/Cu_2O$ nanocomposite anodes with various structures were prepared by different methods and exhibited relatively outstanding electrochemical performance. The synergetic effect of the components of CuO and $Cu_2O$ plays an important role in enhancing the rate capability, specific capacity, and cycling stability of these nanocomposite anodes [53–55]. From Figure 2 and Table 3, we could draw the conclusion that the hybridization of the homoatomic transition metal chalcogenides can effectively enhance the electrochemical performance of a single pure transition metal chalcogenide [45,49].

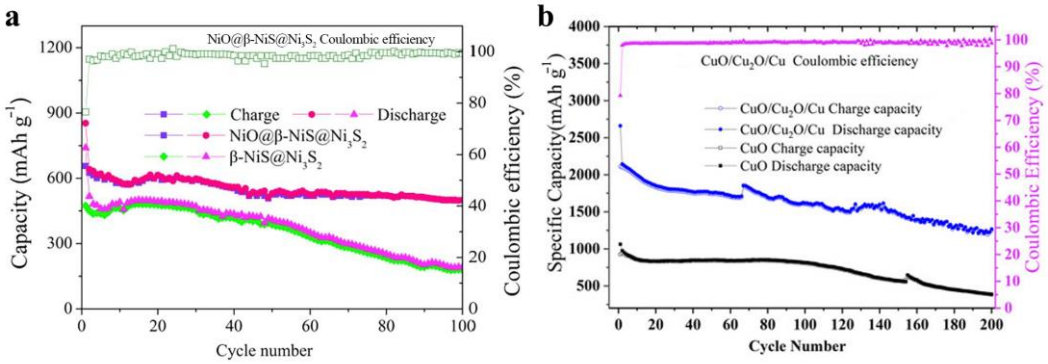



**Figure 2.** (**a**) Comparison of the $NiO@\beta\text{-}NiS@Ni_3S_2$ and $\beta\text{-}NiS@Ni_3S_2$ electrodes at 500 mA/g [45]. (**b**) Comparison of $CuO/Cu_2O/Cu$ and CuO nanowires nanocomposites at 200 mA/g [49].

**Table 3.** The electrochemical performance comparison of X-Chalcogenide and X-Chalcogenide hybrid materials and pure materials.

| Hybrid Materials Capacity [mAh $g^{-1}$] | | Pure Materials Capacity [mAh $g^{-1}$] | | Current [mA $g^{-1}$] | Refs. |
|---|---|---|---|---|---|
| $Co_3O_4@CoO$ | 892 (200 cycles) | $Co_3O_4$ | 425 (200 cycles) | 500 | [41] |
| $Co(OH)_2/Co_3O_4/Co$ | 543 (300 cycles) | $Co_3O_4/Co$ | 200 (100 cycles) | 100 | [42] |
| $MnO/Mn_3O_4/SeO_x$ | 1007 (630 cycles) | $Mn_3O_4/SeO_x$ | 544 (300 cycles) | 1000 | [44] |
| $NiO@NiS@Ni_3S_2$ | 498 (100 cycles) | $NiS@Ni_3S_2$ | 175 (100 cycles) | 500 | [45] |
| $Cu_2O@CuO@RGO$ | 516 (60 cycles) | $Cu_2O@RGO$ | 282 (60 cycles) | 0.1 C | [47] |
| $CuO/Cu_2O/Cu$ | 1266 (200 cycles) | CuO | 385 (200 cycles) | 50 | [49] |
| $CuO/Cu_2O/Cu$ | 534 (100 cycles) | $Cu_2O/Cu$ | 297 (100 cycles) | 100 | [51] |

### *3.2. Hybridization of X-Chalcogenide and Y-Chalcogenide*

The hybridization of different transition metal-based chalcogenides, i.e., X-metal chalcogenide and Y-metal chalcogenide, was widely investigated and could be easily achieved by many different preparation methods. The electrochemical performance of the composites of binary or ternary transition metal-based chalcogenides was almost better than that of each transition metal-based chalcogenide because of the synergetic effect of the components. The hybridization of transition metal chalcogenides could effectively enhance the advantages of a single component at certain concentrations.

A hierarchical $Fe_3O_4$/CuO hybrid wire showed high capacities, excellent rate capabilities, and ultrafast diffusion of Li ions, which was much better than the pure $Fe_3O_4$ or CuO nanomaterial, respectively, originating from the intelligent integration of the $Fe_3O_4$ and CuO and the unique nanowires structure [56]. Due to the synergetic effect between $Mn_3O_4$ and $Fe_3O_4$ and the unique flower-like structure, the $Mn_3O_4$/$Fe_3O_4$ nanocomposites showed superior lithium ion storage ability than pure $Fe_3O_4$ or $Mn_3O_4$, respectively [57].

Porous $Co_3O_4$/CuO composites also displayed better cycling stability and higher capacities than pure $Co_3O_4$ or CuO electrodes because of the synergetic lithium storage effect of both $Co_3O_4$ and CuO, as well as the porous hierarchical structure [58]. The ratios of Co and Cu could affect the morphologies, structures, and further electrochemical performance of the porous $Co_3O_4$/CuO composites, which indicated the vital role of hybridization to adjust electrochemical properties [58]. Directly grown on Cu foam, the heterostructured CoO/$SiO_2$ exhibited high reversible capacity and good rate capability mainly because of the excellent synergetic effect between the two active materials of CoO and $SiO_2$, and the enhanced conductivity of the 3D copper foam [59]. The binary ZnO/CoO mesoporous microspheres with carbon shells were prepared and delivered a good rate capability and high reversible capacity of 1457 mAh/g after 500 cycles, which was ascribed to the synergetic effect of the two components [60]. Composed of cubic $Co_3O_4$ and rhombus NiO, the flower-like NiO/$Co_3O_4$ composites exhibited a low charge transfer resistance and a high initial discharge capacity, indicating the improved conductivity and electrochemical reaction originated from the two metal cations [61]. For the hybrid nanofibrous $Co_3O_4$/$TiO_2$, the initial discharge capacity was higher than the theoretical capacity of pure $Co_3O_4$ at 50.6% $Co_3O_4$ mass content [62]. The reversible capacity of amorphous hybridized $SnO_2$/$Co_3O_4$ nanoflakes with a certain ratio of Sn and Co was much better than that of pure $Co_3O_4$ and $SnO_2$ electrodes, respectively, which was attributed to the different potentials and working mechanisms of the $SnO_2$ and $Co_3O_4$ [63]. Prepared by facile solvothermal and freeze-dring methods, the 3D structured CoO/ZnO nanoclusters anodes delivered a much higher specific capacity, which indicated an improved electrochemical performance by the synergetic effect of CoO and ZnO components [64]. The $Co_3O_4$/$CeO_2$ heterostructure nanocomposites with different molar ratios of Co/Ce were prepared by a facile microwave assistance method. The excellent cycling stability and high reversible capacity of the 5$Co_3O_4$/$CeO_2$ anodes resulted from the appropriate hybridization of $Co_3O_4$ and $CeO_2$ [65]. Synthesized by a series of chemical reaction processes, the hierarchical mesoporous structured CoO@TiO2@C anodes exhibited much better electrochemical performance than that of pure CoO anodes, which indicated the enhanced effect of the robust $TiO_2$ and amorphous carbon shells [66]. For the NiO/CoO nanoneedles, the enhancement of the electrochemical performance mainly resulted from the structural stability and the volume accommodation because of the interspace between NiO-CoO nanoneedles [67].

The core-shell CuO@ZnO composites with different contents of ZnO were synthesized by a chemical process of depositing ZnO on the CuO surface. Compared to pure CuO materials, the specific CuO@ZnO-6.5% anodes showed much superior electrochemical performance [68]. $Cu_{7.2}S_4$/C was introduced to form the core-shell $Cu_{7.2}S_4$/C@$MoS_2$ nanocomposites, which exhibited long-cycle stability and high specific discharge capacity owing to the special oxidation states of Cu and the improved conductivity by the Cu-rich $Cu_{7.2}S_4$ component [69]. ZnO was introduced to suppress the agglomeration and migration of $Cu_2O$ or Cu particles during the carbonization process, and the molar ratios of Zn to Cu can directly affect the size of the bimetallic oxides. At a certain concentration, the carbon-confined $Cu_2O$/ZnO showed a reversible capacity of up to 476 mAh/g [70]. Porous $Cu_2O$/$Mn_3O_4$ hetero-nanosheets exhibited good cycling stability, high reversible capacity, and competitive rate capability because of the synergetic effect of the two components [71]. The flower-like C@$SnO_2$/$Cu_2O$ nanosheet cluster anodes showed much better storage capacity, rate performance, and cycle stability than pure $SnO_2$ anodes because of the carbon layer, the novel structure, and the synergetic effect between the nanosized $SnO_2$ and $Cu_2O$ [72]. Prepared by a facile dealloying process of MnCoAl, $MnCoO_x$ microspheres

anodes exhibited better rate capability, superior cycling stability, and higher capacities than those of pure $Mn_3O_4$ anodes [73]. Figure 3 exhibited the better electrochemical performance of the hybrid of $Mn_3O_4$ than that of pure $Mn_3O_4$ [57,63], while Figure 4 showed the better electrochemical performance of the hybrid of $SnO_2$ than that of each pure component [72,73], indicating the enhanced electrochemical performance by the hybridization of different transition metal-based chalcogenides.

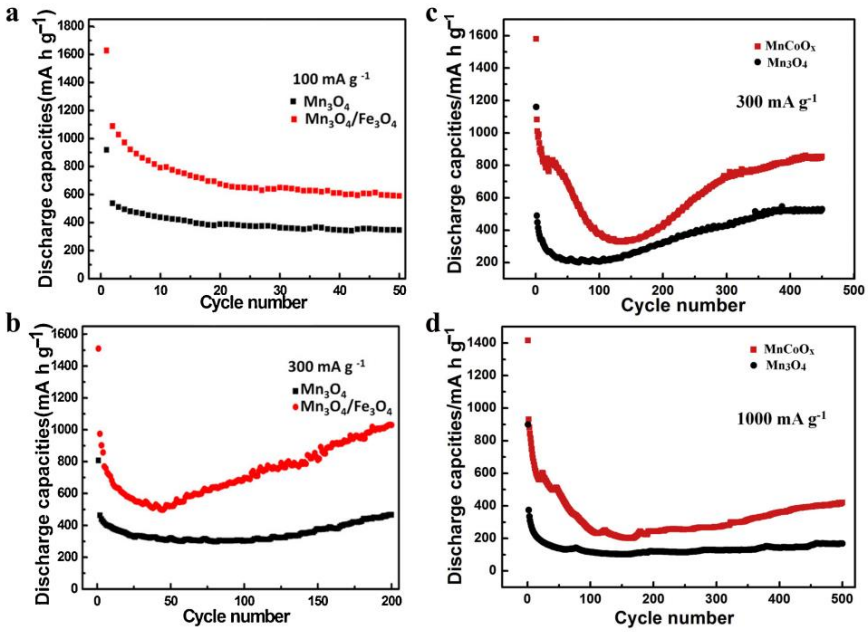



**Figure 3.** Comparison of the $Mn_3O_4/Fe_3O_4$ and $Mn_3O_4$ electrodes at 100 mA/g (**a**) and 300 mA/g (**b**) [57]. Comparison of the $MnCoO_x$ anode and pure $Mn_3O_4$ material at 300 mA/g (**c**) and 1000 mA/g (**d**) [63].

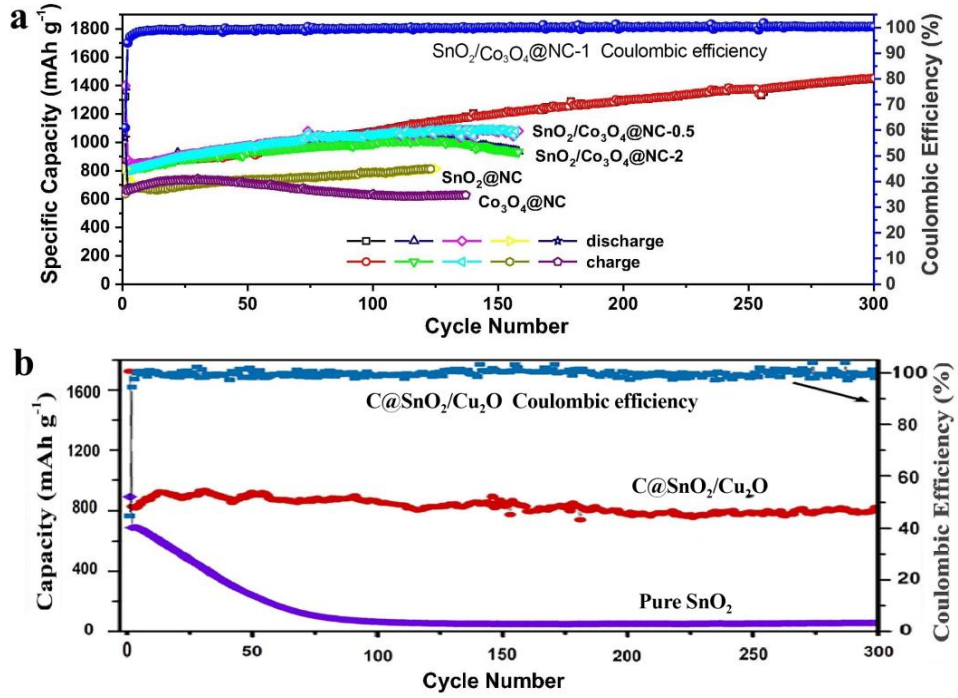



**Figure 4.** (**a**) Comparison of the $SnO_2/Co_3O_4$@NC, $SnO_2$@NC, and $Co_3O_4$@NC electrodes at 200 mA/g [72]. (**b**) Comparison of cycling performance of the C@$SnO_2/Cu_2O$ electrode and pure $SnO_2$ electrode at 0.5 C [73].

Due to the unique architecture and the synergetic effect between the two composites, the bind-free $Co(OH)_2$@$MnO_2$ nanosheets grown on Ni foam showed outstanding electrochemical performance [74]. Multilayer amorphous $SnO_2$ and $TiO_2$ thin films displayed good electrochemical performance due to the heterogeneous structure and the two components. The $SnO_2/TiO_2$ nanocomposite integrated the advantages of the long cycle life of $TiO_2$ and the high specific capacity of $SnO_2$, indicating the enhanced effect of hybridization [75]. The hybrid of transition metal selenides was also synthesized by different methods and exhibited superior electrochemical performance. The CoFeSe/NC anodes exhibited better electrochemical performances (775 mAh $g^{-1}$ after 50 cycles at 0.2 A $g^{-1}$ and 423 mAh $g^{-1}$ at 3 A $g^{-1}$ up to 1000 cycles) and dynamic kinetics than the single-metal selenides, profiting from the synergistic effect of the multi-metal components, and well-retained integrated architecture [76]. Zhang and Pang demonstrated the excellent electrochemical performance of the hybrid of transition metal selenides in energy storage systems, such as lithium-ion batteries, sodium-ion batteries, and supercapacitors, respectively [77,78]. The better electrochemical performance of the hybrid of X-chalcogenide and Y-chalcogenide than pure transition metal chalcogenide was summarized in Table 4.

**Table 4.** The electrochemical performance comparison of X-Chalcogenide and Y-Chalcogenide hybrid materials and pure materials.

| Hybrid Materials Capacity [mAh $g^{-1}$] | | Pure Materials Capacity [mAh $g^{-1}$] | | Current [mA $g^{-1}$] | Refs. |
|---|---|---|---|---|---|
| $Fe_3O_4/CuO$ | 953 (100 cycles) | $Fe_3O_4$ | 260 (100 cycles) | 820 | [56] |
| $Fe_3O_4/CuO$ | 953 (100 cycles) | CuO | 559 (100 cycles) | 820 | [56] |
| $Mn_3O_4/Fe_3O_4$ | 600 (50 cycles) | $Mn_3O_4$ | 400 (50 cycles) | 100 | [57] |
| $Co_3O_4/CuO$ | 800 (80 cycles) | $Co_3O_4$ | 246 (80 cycles) | 100 | [58] |
| $Co_3O_4/CuO$ | 800 (80 cycles) | CuO | 588 (80 cycles) | 100 | [58] |
| $CoO/SiO_2$ | 1251 (250 cycles) | CoO | 752 (50 cycles) | 500 | [59] |
| ZnO-CoO@NC | 1457 (500 cycles) | $ZnCo_2O_4$ | 889 (400 cycles) | 200 | [60] |
| $SnO_2/Co_3O_4$ | 1450 (300 cycles) | $Co_3O_4$ | 625 (135 cycles) | 200 | [63] |
| $SnO_2/Co_3O_4$ | 1450 (300 cycles) | $SnO_2$ | 800 (125 cycles) | 200 | [63] |
| $Co_3O_4/CeO_2$ | 1131 (80 cycles) | $Co_3O_4$ | 539 (100 cycles) | 100 | [65] |
| CoO@$TiO_2$@C | 1136 (200 cycles) | CoO | 17 (100cycles) | 500 | [66] |
| CoO@$TiO_2$@C | 1136 (200 cycles) | $TiO_2$ | 94 (100 cycles) | 500 | [66] |
| CuO@ZnO | 400 (500 cycles) | CuO | 200 (130 cycles) | 0.2 C | [68] |
| $Cu_{7.2}S_4$/C@$MoS_2$ | 1415 (42 cycles) | $MoS_2$ | 254 (42 cycles) | 200 | [69] |
| $Cu_{7.2}S_4$/C@$MoS_2$ | 1527 (340 cycles) | $Cu_{7.2}S_4$/C | 294 (68 cycles) | 1000 | [69] |
| $Cu_2O/Mn_3O_4$ | 792 (350 cycles) | $CuMnO_x$ | 238 (120 cycles) | 2500 | [71] |
| C@$SnO_2/Cu_2O$ | 814 (300 cycles) | $SnO_2$ | 64 (100 cycles) | 0.5 C | [72] |
| $MnCoO_x$ | 860 (450 cycles) | $Mn_3O_4$ | 550 (450 cycles) | 300 | [73] |
| $MnCoO_x$ | 420 (500 cycles) | $Mn_3O_4$ | 168 (500 cycles) | 1000 | [73] |
| $Co(OH)_2$@$MnO_2$ | 700 (150 cycles) | $Co(OH)_2$ | 575 (150 cycles) | 250 | [74] |
| $SnO_2/TiO_2$ | 175 μAhcm$^{-2}$ (200 cycles) | $SnO_2$ | 10 μAhcm$^{-2}$ (200 cycles) | 13.8 μAcm$^{-2}$ | [75] |

## 4. Discussion and Prospect

As is shown in Tables 1–4 and Figures 1–4, the electrochemical performance of hybrid anode materials was always better than that of pure anode materials. Hybridization is an effective method to improve the electrochemical performance of transition metal chalcogenides. Some researchers ascribe the enhanced mechanism of hybridization to the synergetic effect of the different components [64–66], while some researchers believe the interspace of the different phases plays an important role [67]. However, the details of the enhanced mechanism or the synergetic effect have not been further investigated. Based on the experimental results, a suitable theoretical calculation model should be established, and the enhanced mechanism should be deeply studied by using classical molecular dynamics and first-principle calculations in detail. If the interaction of different atoms or different phases is explored clearly, transition metal chalcogenides with excellent electrochemical performance will be prepared and used as anodes practically.

Till now, the study of hybridization has always focused on the hybridization of different crystal components. The study of amorphous/amorphous and amorphous/crystal hybridization has not been widely explored. The amorphous materials have unique features, such as an isotropic nature and more defects, which could provide more active sites and accommodate the volume expansion during the charge-discharge process [79]. Many molecular dynamics simulations and experimental results indicate that the electrochemical performance of amorphous anodes is better than that of crystal anodes [80,81]. The electrochemical performance of amorphous and crystalline Sn@C composites was compared, and the better electrochemical performance of amorphous anodes was ascribed to the unique features of amorphous structures [82]. A novel amorphous $MoS_2/MoO_3$ anode exhibited high specific capacity and cycling stability [83]. Compared to the crystal CoS anode, amorphous CoS exhibited much higher specific capacity and rate capability [10]. The amorphous CoO buffer was introduced to accommodate the volume expansion of CoO nanosheets, by which the CoO nanosheets/CoO film exhibited better electrochemical performance than CoO nanosheets [12]. Based on the unique features of amorphous structures, it is necessary to study structural hybridization combined with component hybridization, such as amorphous/amorphous and amorphous/crystal, which could accommodate the volume expansion and then improve the electrochemical performance of transition metal chalcogenides.

## 5. Conclusions

Due to the synergetic effect, hybridization is an effective way to enhance the electrochemical performance of transition metal chalcogenides as anodes in lithium-ion batteries. The hybridization could be divided into the hybridization between the transition metal and transition metal-based chalcogenide, and the hybridization between different transition metal-based chalcogenides. The electrochemical performance of a hybrid of transition metal chalcogenides is always better than that of pure transition metal chalcogenides. Though excellent electrochemical performance was obtained through the hybridization by many different preparation methods, the enhanced mechanism should be deeply investigated using classical molecular dynamics and first-principle calculations in the future. According to the unique features of amorphous structures, structural hybridization combined with component hybridization, such as amorphous/amorphous and amorphous/crystal, should be further investigated to improve the electrochemical performance. After a thorough understanding of the enhanced mechanism of the hybridization, we believe that a well-designed hybrid of transition metal-based chalcogenides is more promising to be used as future anodes of lithium-ion batteries.

**Author Contributions:** All authors listed have made a substantial contribution to this review and approved it for publication. All authors have read and agreed to the published version of the manuscript.

**Funding:** This review was supported by a Project of Shandong Province Higher Educational Science and Technology Program No. J17KA184.

**Institutional Review Board Statement:** Not applicable.

**Informed Consent Statement:** Not applicable.

**Data Availability Statement:** Not applicable.

**Conflicts of Interest:** The authors declare no conflict of interest.

## References

1. Hu, H.; Li, Q.; Li, L.; Teng, X.; Feng, Z.; Zhang, Y.; Wu, M.; Qiu, J. Laser Irradiation of Electrode Materials for Energy Storage and Conversion. *Matter* **2020**, *3*, 95–126. [CrossRef]
2. Li, H.; Hu, Z.; Xia, Q.; Zhang, H.; Li, Z.; Wang, H.; Li, X.; Zuo, F.; Zhang, F.; Wang, X.; et al. Operando Magnetometry Probing the Charge Storage Mechanism of CoO Lithium-Ion Batteries. *Adv. Mater.* **2021**, *33*, 2006629. [CrossRef] [PubMed]
3. Li, Q.; Li, H.; Xia, Q.; Hu, Z.; Zhu, Y.; Yan, S.; Ge, C.; Zhang, Q.; Wang, X.; Shang, X.; et al. Extra storage capacity in transition metal oxide lithium-ion batteries revealed by in situ magnetometry. *Nat. Mater.* **2021**, *20*, 76–83. [CrossRef] [PubMed]

4. Li, Z.; Zhang, Y.; Li, X.; Gu, F.; Zhang, L.; Liu, H.; Xia, Q.; Li, Q.; Ye, W.; Ge, C.; et al. Reacquainting the Electrochemical Conversion Mechanism of $FeS_2$ Sodium-Ion Batteries by Operando Magnetometry. *J. Am. Chem. Soc.* **2021**, *143*, 12800–12808. [CrossRef]
5. Zhao, Z.; Hu, Z.; Jiao, R.; Tang, Z.; Dong, P.; Li, Y.; Li, S.; Li, H. Tailoring multi-layer architectured $FeS_2$@C hybrids for superior sodium-, potassium- and aluminum-ion storage. *Energy Storage Mater.* **2019**, *22*, 228–234. [CrossRef]
6. Zhao, Z.; Hu, Z.; Li, Q.; Li, H.; Zhang, X.; Zhuang, Y.; Wang, F.; Yu, G. Designing two-dimensional $WS_2$ layered cathode for high-performance aluminum-ion batteries: From micro-assemblies to insertion mechanism. *Nano Today* **2020**, *32*, 100870. [CrossRef]
7. Chu, D.B.; Li, J.; Yuan, X.M.; Li, Z.L.; Wei, X.; Wan, Y. Tin-Based Alloy Anode Materials for Lithium Ion Batteries. *Prog. Chem.* **2012**, *24*, 1466–1476.
8. Feng, Z.-Y.; Peng, W.-J.; Wang, Z.-X.; Guo, H.-J.; Li, X.-H.; Yan, G.-C.; Wang, J.-X. Review of silicon-based alloys for lithium-ion battery anodes. *Int. J. Miner. Metall. Mater.* **2021**, *28*, 1549–1564. [CrossRef]
9. Adams, J.N.; Nelson, G.J. Cycling-Induced Microstructural Changes in Alloy Anodes for Lithium-Ion Batteries. *J. Electrochem. Energy Convers. Storage* **2021**, *18*, 1–33. [CrossRef]
10. Ren, L.-L.; Wang, L.-H.; Qin, Y.-F.; Li, Q. One-Pot Synthesized Amorphous Cobalt Sulfide With Enhanced Electrochemical Performance as Anodes for Lithium-Ion Batteries. *Front. Chem.* **2022**, *9*, 1186. [CrossRef]
11. Wang, L.-H.; Ren, L.-L.; Qin, Y.-F.; Li, Q. Hydrothermal Preparation and High Electrochemical Performance of NiS Nanospheres as Anode for Lithium-Ion Batteries. *Front. Chem.* **2022**, *9*, 1210. [CrossRef]
12. Wang, L.-H.; Teng, X.-L.; Qin, Y.-F.; Li, Q. High electrochemical performance and structural stability of CoO nanosheets/CoO film as self-supported anodes for lithium-ion batteries. *Ceram. Int.* **2021**, *47*, 5739–5746. [CrossRef]
13. Chen, Y.; Li, J.; Lei, Z.; Huo, Y.; Yang, L.; Zeng, S.; Ding, H.; Qin, Y.; Jie, Y.; Huang, F.; et al. Hollow CuS Nanoboxes as Li-Free Cathode for High-Rate and Long-Life Lithium Metal Batteries. *Adv. Energy Mater.* **2020**, *10*, 1903401. [CrossRef]
14. Zhou, M.; Peng, N.; Liu, Z.; Xi, Y.; He, H.; Xia, Y.; Liu, Z.; Okada, S. Synthesis of sub-10 nm copper sulphide rods as high-performance anode for long-cycle life Li-ion batteries. *J. Power Sources* **2016**, *306*, 408–412. [CrossRef]
15. Zhao, L.; Tao, F.; Quan, Z.; Zhou, X.; Yuan, Y.; Hu, J. Bubble template synthesis of copper sulfide hollow spheres and their applications in lithium ion battery. *Mater. Lett.* **2012**, *68*, 28–31. [CrossRef]
16. Li, Z.; Li, G.; Xu, W.; Zhou, M.; Xu, C.; Shi, M.; Li, F.; Chen, L.; He, B. Self-Integrated Porous Leaf-like CuO Nanoplate Array-Based Anodes for High-Performance Lithium-Ion Batteries. *ChemElectroChem* **2018**, *5*, 2774–2780. [CrossRef]
17. Han, D.; Xiao, N.; Liu, B.; Song, G.; Ding, J. One-pot synthesis of core/shell-structured NiS@onion-like carbon nanocapsule as a high-performance anode material for Lithium-ion batteries. *Mater. Lett.* **2017**, *196*, 119–122. [CrossRef]
18. Guo, S.P.; Li, J.C.; Xiao, J.R.; Xue, H.G. $Fe_3S_4$ Nanoparticles Wrapped in an rGO Matrix for Promising Energy Storage: Outstanding Cyclic and Rate Performance. *ACS Appl. Mater. Interfaces* **2017**, *9*, 37694–37701. [CrossRef]
19. Han, F.; Li, W.-C.; Li, D.; Lu, A.-H. In Situ Electrochemical Generation of Mesostructured $Cu_2S$/C Composite for Enhanced Lithium Storage: Mechanism and Material Properties. *ChemElectroChem* **2014**, *1*, 733–740. [CrossRef]
20. Liu, H.; Zhou, W.; Zhang, Y. One-pot Solvothermal Synthesis of CuS-CNTs Hybrid as Binder-free Anode Material for Lithium Ion Batteries. *Colloid Interface Sci. Commun.* **2016**, *15*, 1–4. [CrossRef]
21. Mai, Y.J.; Wang, X.L.; Xiang, J.Y.; Qiao, Y.Q.; Zhang, D.; Gu, C.D.; Tu, J.P. CuO/graphene composite as anode materials for lithium-ion batteries. *Electrochim. Acta* **2011**, *56*, 2306–2311. [CrossRef]
22. Varghese, S.P.; Babu, B.; Prasannachandran, R.; Antony, R.; Shaijumon, M.M. Enhanced electrochemical properties of $Mn_3O_4$/graphene nanocomposite as efficient anode material for lithium ion batteries. *J. Alloys Compd.* **2019**, *780*, 588–596. [CrossRef]
23. Wu, L.-L.; Zhao, D.-L.; Cheng, X.-W.; Ding, Z.-W.; Hu, T.; Meng, S. Nanorod $Mn_3O_4$ anchored on graphene nanosheet as anode of lithium ion batteries with enhanced reversible capacity and cyclic performance. *J. Alloys Compd.* **2017**, *728*, 383–390. [CrossRef]
24. Zhang, L.; Hu, P.; Zhao, X.; Tian, R.; Zou, R.; Xia, D. Controllable synthesis of core–shell Co@CoO nanocomposites with a superior performance as an anode material for lithium-ion batteries. *J. Mater. Chem.* **2011**, *21*, 18279–18283. [CrossRef]
25. Sun, X.; Hao, G.-P.; Lu, X.; Xi, L.; Liu, B.; Si, W.; Ma, C.; Liu, Q.; Zhang, Q.; Kaskel, S.; et al. High-defect hydrophilic carbon cuboids anchored with Co/CoO nanoparticles as highly efficient and ultra-stable lithium-ion battery anodes. *J. Mater. Chem. A* **2016**, *4*, 10166–10173. [CrossRef]
26. Sun, M.; Zhang, H.; Wang, Y.-F.; Liu, W.-L.; Ren, M.-M.; Kong, F.-G.; Wang, S.-J.; Wang, X.-Q.; Duan, X.-L.; Ge, S.-Z. Co/CoO@N-C nanocomposites as high-performance anodes for lithium-ion batteries. *J. Alloys Compd.* **2019**, *771*, 290–296. [CrossRef]
27. Xu, D.; Mu, C.; Xiang, J.; Wen, F.; Su, C.; Hao, C.; Hu, W.; Tang, Y.; Liu, Z. Carbon-Encapsulated $Co_3O_4$ @CoO@Co Nanocomposites for Multifunctional Applications in Enhanced Long-life Lithium Storage, Supercapacitor and Oxygen Evolution Reaction. *Electrochim. Acta* **2016**, *220*, 322–330. [CrossRef]
28. Chen, R.; Wang, Y.; Nuli, Y.; Yu, Y.; Gao, P.; Chen, Q.; Wei, L.; Hu, N.; Yang, Z.; Gao, R.; et al. $Cu_2O$ nanowires as anode materials for Li-ion rechargeable batteries. *Sci. China Technol. Sci.* **2014**, *57*, 1073–1076. [CrossRef]
29. Zhou, H.; Zhao, H.; Zhang, X.; Cheng, H.; Lu, X.; Xu, Q. Facile one-step synthesis of Cu2O@Cu sub-microspheres composites as anode materials for lithium ion batteries. *J. Mater. Sci. Technol.* **2018**, *34*, 1085–1090. [CrossRef]
30. Wang, Y.; Cao, L.; Li, J.; Kou, L.; Huang, J.; Feng, Y.; Chen, S. Cu/$Cu_2O$@Ppy nanowires as a long-life and high-capacity anode for lithium ion battery. *Chem. Eng. J.* **2020**, *391*, 123597. [CrossRef]

31. Ni, S.; Yang, X.; Li, T. Fabrication of a porous NiS/Ni nanostructured electrode via a dry thermal sulfuration method and its application in a lithium ion battery. *J. Mater. Chem.* **2012**, *22*, 2395–2397. [CrossRef]
32. Liu, H.; Hu, R.; Sun, W.; Zeng, M.; Liu, J.; Yang, L.; Zhu, M. Sn@$SnO_x$/C nanocomposites prepared by oxygen plasma-assisted milling as cyclic durable anodes for lithium ion batteries. *J. Power Sources* **2013**, *242*, 114–121. [CrossRef]
33. Chen, C.; Huang, Y.; Zhang, H.; Wang, X.; Wang, Y.; Jiao, L.; Yuan, H. Controllable synthesis of Cu-doped CoO hierarchical structure for high performance lithium-ion battery. *J. Power Sources* **2016**, *314*, 66–75. [CrossRef]
34. Han, X.; Cui, Y.; Liu, H. Ce-doped $Mn_3O_4$ as high-performance anode material for lithium ion batteries. *J. Alloys Compd.* **2020**, *814*, 152348. [CrossRef]
35. Kumar, P.S.M.; Al-Muhtaseb, A.H.; Kumar, G.; Vinu, A.; Cha, W.; Cab, J.V.; Pal, U.; Krishnan, S.K. Piper longum Extract-Mediated Green Synthesis of Porous $Cu_2O$:Mo Microspheres and Their Superior Performance as Active Anode Material in Lithium-Ion Batteries. *ACS Sustain. Chem. Eng.* **2020**, *8*, 14557–14567. [CrossRef]
36. Liang, J.; Kong, J.; Zhang, J. Hollow Concave Zinc-Doped $Co_3O_4$ Nanosheets/Carbon Composites as Ultrahigh Capacity Anode Materials for Lithium-Ion Batteries. *Chemelectrochem* **2021**, *8*, 172–178. [CrossRef]
37. Lee, J.; Zhu, H.; Deng, W.; Wu, Y. Synthesis of $Cu_{3.8}$Ni/CoO and $Cu_{3.8}$Ni/MnO nanoparticles for advanced lithium-ion battery anode materials. *Nano Res.* **2016**, *10*, 1033–1043. [CrossRef]
38. Zhang, Z.; Yin, L. Mn-doped $Co_2(OH)_3Cl$ xerogels with 3D interconnected mesoporous structures as lithium ion battery anodes with improved electrochemical performance. *J. Mater. Chem. A* **2015**, *3*, 17659–17668. [CrossRef]
39. Chen, W.; Kuang, S.; Liu, Z.; Fu, H.; Yun, Q.; Xu, D.; Hu, H.; Yu, X. Y-doped $Li_4Ti_{5-x}Y_xO_{12}$ with $Y_2Ti_2O_7$ surface modification anode materials: Superior rate capability and ultra long cyclability for half/full lithium-ion batteries. *J. Alloys Compd.* **2020**, *835*, 155327–155336. [CrossRef]
40. Huang, R.; Zhou, R.; Wang, L.; Zhu, Y. Dandelion-like CoO/$Co_3O_4$/Carbon Composites as Anode Materials for a High-Performance Lithium Ion Battery. *ChemistrySelect* **2020**, *5*, 12932–12939. [CrossRef]
41. Liu, Y.G.; Zhang, H.Z.; Jiang, N.; Zhang, W.X.; Arandiyan, H.; Wang, Z.Y.; Luo, S.H.; Fang, F.; Sun, H.Y. Porous $Co_3O_4$@CoO composite nanosheets as improved anodes for lithium-ion batteries. *J. Alloys Compd.* **2020**, *834*, 8. [CrossRef]
42. Li, J.-X.; Xie, Q.; Zhao, P.; Li, C. EDTA-Co(II) sodium complex derived $Co(OH)_2$/$Co_3O_4$/Co nanoparticles embedded in nitrogen-enriched graphitic porous carbon as lithium-ion battery anode with superior cycling stability. *Appl. Surf. Sci.* **2020**, *504*, 144515. [CrossRef]
43. Zhou, X.; Long, B.; Cheng, F.; Tang, J.; Sun, A.; Yang, J.; Jia, M.; Wang, H. N-doped carbon encapsulated porous MnO/Mn3O4 submicrospheres as high-performance anode for lithium-ion batteries. *J. Electroanal. Chem.* **2019**, *838*, 1–6. [CrossRef]
44. Li, L.-W.; Wang, L.-P.; Zhang, M.-Y.; Huang, Q.-Z.; He, K.-J.; Wu, F.-X. Enhancement of lithium storage capacity and rate performance of Se-modified MnO/$Mn_3O_4$ hybrid anode material via pseudocapacitive behavior. *Trans. Nonferrous Met. Soc. China* **2020**, *30*, 1904–1915. [CrossRef]
45. Wu, X.; Li, S.; Xu, Y.; Wang, B.; Liu, J.; Yu, M. Hierarchical heterostructures of NiO nanosheet arrays grown on pine twig-like β-NiS@$Ni_3S_2$ frameworks as free-standing integrated anode for high-performance lithium-ion batteries. *Chem. Eng. J.* **2019**, *356*, 245–254. [CrossRef]
46. Wang, L.-H.; Dai, Y.-K.; Qin, Y.-F.; Chen, J.; Zhou, E.-L.; Li, Q.; Wang, K. One-Pot Synthesis and High Electrochemical Performance of CuS/$Cu_{1.8}$S Nanocomposites as Anodes for Lithium-Ion Batteries. *Materials* **2020**, *13*, 3797. [CrossRef] [PubMed]
47. Pu, F.; Bai, Y.; Lv, J.; Zhao, X.; Wu, G.; Kong, C.; Lei, B.; Zhang, X.; Jin, H.; Yang, Z. Yolk–Shell $Cu_2O$@CuO-decorated RGO for High-Performance Lithium-Ion Battery Anode. *Energy Environ. Mater.* **2022**, *5*, 253–260. [CrossRef]
48. Li, Z.; Xie, G.; Wang, C.; Liu, Z.; Chen, J.; Zhong, S. Binder free $Cu_2O$/CuO/Cu/Carbon-polymer composite fibers derived from metal/organic hybrid materials through electrodeposition method as high performance anode materials for lithium-ion batteries. *J. Alloys Compd.* **2021**, *864*, 158585. [CrossRef]
49. Wang, L.-H.; Gao, S.; Ren, L.-L.; Zhou, E.-L.; Qin, Y.-F. The Synergetic Effect Induced High Electrochemical Performance of CuO/$Cu_2O$/Cu Nanocomposites as Lithium-Ion Battery Anodes. *Front. Chem.* **2021**, *9*, 1035. [CrossRef] [PubMed]
50. Xu, C.; Manukyan, K.V.; Adams, R.A.; Pol, V.G.; Chen, P.; Varma, A. One-step solution combustion synthesis of CuO/$Cu_2O$/C anode for long cycle life Li-ion batteries. *Carbon* **2019**, *142*, 51–59. [CrossRef]
51. Liu, S.; Hou, H.; Liu, X.; Duan, J.; Yao, Y.; Liao, Q. High-performance hierarchical cypress-like CuO/$Cu_2O$/Cu anode for lithium ion battery. *Ionics* **2016**, *23*, 1075–1082. [CrossRef]
52. Kim, A.Y.; Kim, M.K.; Cho, K.; Woo, J.Y.; Lee, Y.; Han, S.H.; Byun, D.; Choi, W.; Lee, J.K. One-Step Catalytic Synthesis of CuO/$Cu_2O$ in a Graphitized Porous C Matrix Derived from the Cu-Based Metal-Organic Framework for Li- and Na-Ion Batteries. *ACS Appl. Mater. Interfaces* **2016**, *8*, 19514–19523. [CrossRef]
53. Zhao, Y.; Zhang, Y.; Zhao, H.; Li, X.; Li, Y.; Wen, L.; Yan, Z.; Huo, Z. Epitaxial growth of hyperbranched Cu/$Cu_2O$/CuO core-shell nanowire heterostructures for lithium-ion batteries. *Nano Res.* **2015**, *8*, 2763–2776. [CrossRef]
54. Zhou, X.; Shi, J.; Liu, Y.; Su, Q.; Zhang, J.; Du, G. Microwave-assisted synthesis of hollow CuO–$Cu_2O$ nanosphere/graphene composite as anode for lithium-ion battery. *J. Alloys Compd.* **2014**, *615*, 390–394. [CrossRef]
55. Hu, L.; Huang, Y.; Zhang, F.; Chen, Q. CuO/$Cu_2O$ composite hollow polyhedrons fabricated from metal-organic framework templates for lithium-ion battery anodes with a long cycling life. *Nanoscale* **2013**, *5*, 4186–4190. [CrossRef] [PubMed]
56. Saadat, S.; Zhu, J.; Sim, D.H.; Hng, H.H.; Yazami, R.; Yan, Q. Coaxial $Fe_3O_4$/CuO hybrid nanowires as ultra fast charge/discharge lithium-ion battery anodes. *J. Mater. Chem. A* **2013**, *1*, 8672–8678. [CrossRef]

57. Zhao, D.; Hao, Q.; Xu, C. Facile fabrication of composited $Mn_3O_4/Fe_3O_4$ nanoflowers with high electrochemical performance as anode material for lithium ion batteries. *Electrochim. Acta* **2015**, *180*, 493–500. [CrossRef]
58. Shi, L.; Fan, C.; Fu, X.; Yu, S.; Qian, G.; Wang, Z. Carbonate-assisted hydrothermal synthesis of porous hierarchical $Co_3O_4/CuO$ composites as high capacity anodes for lithium-ion batteries. *Electrochim. Acta* **2016**, *197*, 23–31. [CrossRef]
59. Hou, S.; Liao, M.; Guo, Y.; Liu, T.; Wang, L.; Li, J.; Mei, C.; Fu, W.; Zhao, L. $SiO_2$ nanoparticles modulating the "flos albiziae" like CoO by the synergistic effect with enhanced lithium storage. *Appl. Surf. Sci.* **2020**, *530*, 147223. [CrossRef]
60. Liu, J.; Wu, J.; Zhou, C.; Zhang, P.; Guo, S.; Li, S.; Yang, Y.; Li, K.; Chen, L.; Wang, M. Single-phase $ZnCo_2O_4$ derived ZnO–CoO mesoporous microspheres encapsulated by nitrogen-doped carbon shell as anode for high-performance lithium-ion batteries. *J. Alloys Compd.* **2020**, *825*, 153951. [CrossRef]
61. Liu, Q.; Zheng, G.X.; Yin, J.H.; Song, M.X.; Wang, Y.; Tian, S.Y.; Zhang, F.Q. A Flower-Shape $NiO/Co_3O_4$ Composite as Anode for Lithium Ion Battery Prepared by a Template-Free Hydrothermal Method. *Int. J. Electrochem. Sci.* **2020**, *15*, 11522–11530. [CrossRef]
62. Wang, F.; Yuan, H.; Huang, J.G. A bio-inspired nanofibrous $Co_3O_4/TiO_2$/carbon composite as high-performance anodic material for lithium-ion batteries. *J. Alloys Compd.* **2020**, *819*, 12. [CrossRef]
63. Wang, J.K.; Wang, H.K.; Yao, T.H.; Liu, T.; Tian, Y.P.; Li, C.; Li, F.; Meng, L.J.; Cheng, Y.H. Porous N-doped carbon nanoflakes supported hybridized $SnO_2/Co_3O_4$ nanocomposites as high-performance anode for lithium-ion batteries. *J. Colloid Interface Sci.* **2020**, *560*, 546–554. [CrossRef]
64. Yan, Z.; Sun, Z.; Yue, K.; Li, A.; Qian, L. CoO/ZnO nanoclusters immobilized on N-doped 3D reduced graphene oxide for enhancing lithium storage capacity. *J. Alloys Compd.* **2020**, *836*, 155443. [CrossRef]
65. Kang, Y.; Zhang, Y.H.; Shi, Q.; Shi, H.W.; Xue, D.F.; Shi, F.N. Highly efficient $Co_3O_4/CeO_2$ heterostructure as anode for lithium-ion batteries. *J. Colloid Interface Sci.* **2021**, *585*, 705–715. [CrossRef]
66. Yuan, Y.F.; Zhao, W.C.; Chen, L.; Cai, G.S.; Guo, S.Y. CoO hierarchical mesoporous nanospheres@$TiO_2$@C for high-performance lithium-ion storage. *Appl. Surf. Sci.* **2021**, *556*, 149810. [CrossRef]
67. Wei, Y.; Yan, F.; Tang, X.; Luo, Y.; Zhang, M.; Wei, W.; Chen, L. Solvent-Controlled Synthesis of NiO–CoO/Carbon Fiber Nanobrushes with Different Densities and Their Excellent Properties for Lithium Ion Storage. *ACS Appl. Mater. Interfaces* **2015**, *7*, 21703–21711. [CrossRef]
68. Liu, B.; Yongming, C.; Yinyin, Z.; Jiajiao, A.; Haiyun, C.; Tasawar, H.; Ahmed, A.; Bashir, A. The Preparation of CuO@ZnO Core-Shell Materials as High- Stability Anodes for Lithium-Ion Batteries. *Int. J. Electrochem. Sci.* **2019**, *14*, 8973–8985. [CrossRef]
69. Liu, Z.; Qi, S.; Liu, G.; Cheng, L.; Chen, J.; Lou, Y. 3D Metal-Rich $Cu_{7.2}S_4$/Carbon-Supported $MoS_2$ Nanosheets for Enhanced Lithium-Storage Performance. *ChemElectroChem* **2019**, *6*, 1458–1465. [CrossRef]
70. Nie, Y.; Wang, F.; Zhang, H.; Wei, D.; Zhong, S.; Wang, L.; Zhang, G.; Duan, H.; Cao, R. Tunable confinement of Cu-Zn bimetallic oxides in carbon nanofiber networks by thermal diffusion for lithium-ion battery. *Appl. Surf. Sci.* **2020**, *517*, 146079. [CrossRef]
71. Pan, Y.; Xu, M.; Yang, L.; Yu, M.; Liu, H.; Zeng, F. Porous architectures assembled with ultrathin $Cu_2O$–$Mn_3O_4$ hetero-nanosheets vertically anchoring on graphene for high-rate lithium-ion batteries. *J. Alloys Compd.* **2020**, *819*, 152969. [CrossRef]
72. Wang, M.; Zhang, X.; He, X.; Zhu, B.; Tang, H.; Wang, C. In-Situ grown flower-like C@$SnO_2/Cu_2O$ nanosheet clusters on Cu foam as high performance anode for lithium-ion batteries. *J. Alloys Compd.* **2021**, *856*, 158202. [CrossRef]
73. Ye, J.; Zhao, D.; Hao, Q.; Xu, C. Facile Fabrication of Hierarchical Manganese-Cobalt Mixed Oxide Microspheres as High-Performance Anode Material for Lithium Storage. *Electrochim. Acta* **2016**, *222*, 1402–1409. [CrossRef]
74. Kundu, M.; Singh, G.; Svensson, A.M. $Co(OH)_2$@$MnO_2$ nanosheet arrays as hybrid binder-free electrodes for high-performance lithium-ion batteries and supercapacitors. *New J. Chem.* **2019**, *43*, 1257–1266. [CrossRef]
75. Fan, S.; Zhang, J.; Teng, X.; Wang, X.; Li, H.; Li, Q.; Xu, J.; Cao, D.; Li, S.; Hu, H. Self-Supported Amorphous $SnO_2/TiO_2$ Nanocomposite Films with Improved Electrochemical Performance for Lithium-Ion Batteries. *J. Electrochem. Soc.* **2019**, *166*, A3072–A3078. [CrossRef]
76. Li, Z.; Hu, X.; Zhang, Y.; Zhang, W.; Meng, Q.; Tang, S.; Li, D.; Shi, Z.; Wang, Z. Multi-scale study on a synergetic multimetal-based selenide anode with nitrogen-doped porous carbon support for high-performance lithium storage. *J. Alloys Compd.* **2022**, *919*, 165841. [CrossRef]
77. Hussain, I.; Sahoo, S.; Lamiel, C.; Nguyen, T.T.; Ahmed, M.; Xi, C.; Iqbal, S.; Ali, A.; Abbas, N.; Javed, M.S.; et al. Research progress and future aspects: Metal selenides as effective electrodes. *Energy Storage Mater.* **2022**, *47*, 13–43. [CrossRef]
78. Zhou, H.; Li, X.; Li, Y.; Zheng, M.; Pang, H. Applications of M(x)Se(y) (M = Fe, Co, Ni) and Their Composites in Electrochemical Energy Storage and Conversion. *Nano-Micro Lett.* **2019**, *11*, 40. [CrossRef]
79. Hou, L.; Cui, R.; Jiang, X.; Wang, D.; Jiang, Y.; Deng, S.; Guo, Y.; Gao, F. Unique amorphous manganese oxide/rGo anodes for lithium-ion batteries with high capacity and excellent stability. *Ionics* **2020**, *26*, 4339–4349. [CrossRef]
80. Zeng, T.; Zhang, C. Facile-synthesized amorphous $CoCO_3$ for high-capacity lithium-ion battery anode. *Ionics* **2019**, *25*, 4149–4159. [CrossRef]
81. Lim, S.-Y.; Jang, W.; Yun, S.; Yoon, W.-S.; Choi, J.-Y.; Whang, D. Amorphous germanium oxide nanobubbles for lithium-ion battery anode. *Mater. Res. Bull.* **2019**, *110*, 24–31. [CrossRef]

82. Duan, Y.; Du, S.; Tao, H.; Yang, X. Sn@C composite for lithium ion batteries: Amorphous vs. crystalline structures. *Ionics* **2021**, *27*, 1403–1412. [CrossRef]
83. Zhu, K.; Wang, X.; Liu, J.; Li, S.; Wang, H.; Yang, L.; Liu, S.; Xie, T. Novel Amorphous $MoS_2$/$MoO_3$/Nitrogen-Doped Carbon Composite with Excellent Electrochemical Performance for Lithium Ion Batteries and Sodium Ion Batteries. *ACS Sustain. Chem. Eng.* **2017**, *5*, 8025–8034. [CrossRef]

**Disclaimer/Publisher's Note:** The statements, opinions and data contained in all publications are solely those of the individual author(s) and contributor(s) and not of MDPI and/or the editor(s). MDPI and/or the editor(s) disclaim responsibility for any injury to people or property resulting from any ideas, methods, instructions or products referred to in the content.